JOURNAL OF PROPULSION AND POWER
Vol. 30, No. 1, January–February 2014

Combustion of Frozen Nanoaluminum and Water Mixtures

Grant A. Risha,* Terrence L. Connell, Jr.,† and Richard A. Yetter‡
Pennsylvania State University, University Park, Pennsylvania 16801
and
Dilip S. Sundaram§ and Vigor Yang¶
Georgia Institute of Technology, Atlanta, Georgia 30332

DOI: 10.2514/1.B34783

Steady-state strand burner and laboratory-scale static fire motor experiments were used to determine the relative performance and viability of an environmentally friendly solid propellant composed of only nanoaluminum and frozen water. The nominal size of the nanoaluminum particles was 80 nm. The particles were homogeneously mixed with water to form pastes or colloids and then frozen. The measured parameters include burning rates, slag accumulation, thrust, and pressure. A system scaling study was performed to examine the effect of the size of the small-scale motors. The equivalence ratio was fixed at 0.71 for the strand burner and the laboratory-scale motor experiments. The effect of pressure on the linear burning rate was also examined. For an equivalence ratio of 0.71, the mixture exhibited a linear burning rate of 4.8 cm/s at a pressure of 10.7 MPa and a pressure exponent of 0.79. Three motors of internal diameters in the range of 1.91–7.62 cm were studied. Grain configuration, nozzle throat diameter, and igniter strength were varied. The propellants were successfully ignited and combusted in each laboratory-scale motor, generating thrust levels above 992 N in the 7.62-cm-diam motor with a center-perforated grain configuration (7.62 cm length) and an expansion ratio of 10. For the 7.62 cm motor, combustion efficiency was 69%, whereas the specific impulse efficiency was 64%. Increased combustion efficiency and improved ease of ignition were observed at higher chamber pressures (greater than 8 MPa).

I. Introduction

ALUMINUM–WATER combustion has been studied since the 1960s [1–7] as a powerful source for propulsion due to its large amount of energy release as well as green exhaust products [8–11]. In addition to applications for underwater propulsion, the simplicity and storability of Al-H_2O propellants make them viable candidates for space propulsion in low Earth orbit and even as in situ propellants for lunar and Mars missions. Retaining the combustion products onboard could also be considered if reduction methods were available to regenerate the aluminum fuel during the mission or if the added weight were deemed useful for a particular mission.

Lo et al. examined frozen hydrogen peroxide (H_2O_2) with polyethylene (PE) or hydroxyl-terminated polybutadiene (HTPB) solid propellants, referred to as cryogenic solid propellants (CSPs), for booster or lower stage applications [12]. They studied the burning behaviors of CSPs in a 1 kg sandwich (disk stack) configuration in a pressurized environment in which the fuel modules (varied spacing) were adjacent to H_2O_2 modules and a hydrogen–air diffusion flame was passed over the propellant surface for ignition. Burning rates as a function of pressure for the different CSP formulations were obtained, yielding a pressure exponent of 0.155 to 0.165, which is desirable for rocket applications. Adirim et al. successfully hot-fired rocket motors using CSP disk stacks consisting of solid H_2O_2 and PE where the pressure reached nearly 9 MPa a few seconds after ignition [13,14].

Based upon the CSP concept, Franson et al. replaced a portion or all of the polymeric fuel with metals and metal hydrides [15,16] and referred to these propellants as refrigerated solid propellants (RSPs). Two different types of tests were performed on various RSP formulations using aluminum as the fuel component for all formulations, and both water and a combination of water and hydrogen peroxide were considered as the oxidizer. A total of five RSP compositions were examined, with the water content ranging from 60 to 70% of the mixture. In some cases, nanometer aluminum (nAl) was used to replace a fraction of the micron-sized particles. The first experiment involved a closed bomb configuration to examine the effect of pressure on the burning rate. The RSP material was placed in a 1-cm-diam glass pipe and ignited with a hot wire at the top. The second experiment was a center-perforated (CP) motor firing. A conventional cylindrical Ballistic Test and Evaluation System (BATES) motor was employed. The grain geometry was 86 mm outer diameter, 60 mm inner diameter, and 157 mm length. The nozzle was designed to have a target pressure of 2–3 MPa. The igniter, made of a common composite propellant (HTPB–Al–ammonium perchlorate (AP)), was designed to burn for 4 s. Ignition, however, was not always smooth. The grain ignited and burned, producing a measured pressure of 2 MPa. Approximately 13% residue remained in the chamber after the test run. This suggested that 17% of the aluminum in the RSP did not burn, and, consequently, a lower pressure was achieved than was targeted based upon theoretical calculations.

Recent advances in nanosized energetic particles have enabled their use as major ingredients in propellants with enhanced properties and performance [17–23]. In the current investigation, the performance and viability of nanoaluminum (nAl) and ice (ALICE) propellants were examined. Safety tests such as electrostatic discharge, mechanical tensile tests, and impact tests have been performed and are reported elsewhere [24]. Both steady-state strand burner experiments and laboratory-scale hot-fire motor experiments were employed to obtain ballistics data. Linear and mass burning rates, slag accumulation, effect of motor size, thrust, and pressure

Presented as Paper 2009-4877 at the 45th AIAA/ASME/SAE/ASEE Joint Propulsion Conference and Exhibit, Denver, CO, 2–5 August 2009; received 7 September 2012; revision received 2 May 2013; accepted for publication 23 June 2013; published online 31 December 2013.

*Associate Professor, Division of Business and Engineering; Altoona College, Altoona, PA.
†Research Staff, Department of Mechanical and Nuclear Engineering.
‡Professor, Department of Mechanical and Nuclear Engineering.
§Research Assistant, School of Aerospace Engineering.
¶Willliam R.T. Oakes Professor and Chair, School of Aerospace Engineering.

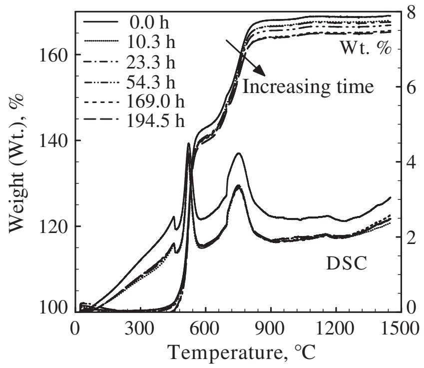

Fig. 1 TGA and DSC of 80 nm aluminum with and without additional passivation.

were measured. The effects of motor scaling on heat loss, slag accumulation, and thrust were examined. Whereas the ideal specific impulse of ALICE propellants depends upon the size of the aluminum particles (due to the thickness of the passivating oxide layer) and equivalence ratio, typical values of I_{sp} and $I_{sp,vac}$ ($P = 1000$ psia, perfect expansion, 74.5 wt% active aluminum) are 207 and 230 s, respectively, considerably lower than conventional AP–HTPB–Al composite propellants in use today (which have I_{sp} of 265 s at $P = 1000$ psia and sea level expansion). Given the simplicity of ALICE propellants, however, the potential for in situ recovery, and the storability of hydrogen in a solid form, further fundamental studies of the combustion processes are reported here.

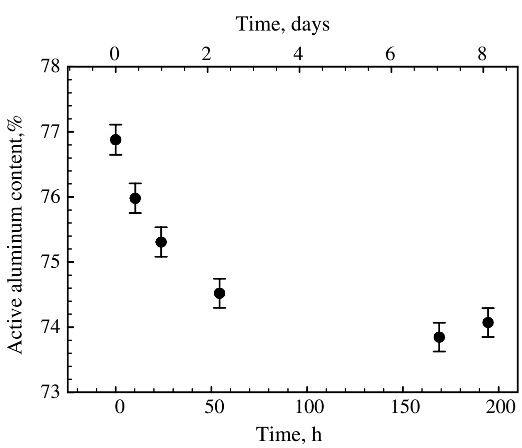

Fig. 2 Active aluminum content as a function of time for extended air passivation of 80 nm aluminum particles.

II. Experimental Approach

Two different experimental facilities were used in this investigation to characterize the combustion and propulsion behavior of ALICE and conventional composite propellants. Each test facility offered unique ballistic information for the family of propellants of concern. The first experiment employed a high-pressure optical strand burner to determine the influence of pressure on propellant burning behaviors. Results served as guidance for the design, construction, and testing of laboratory-scale motors having various grain sizes and configurations. Motor propulsive performance quantities such as thrust and total impulse were then investigated as a function of propellant formulation and grain size/geometry.

A. Materials Characterization

The ALICE propellant formulations used here consisted of nanometer aluminum and deionized water only. The aluminum particles were obtained from Novacentrix and had a nominal diameter of 80 nm. From our previous studies with this material [25–29], particle densities inclusive of the oxide coating, measured using a pycnometer, had values near 3 g/cm^3 (compared with bulk Al of 2.7 g/cm^3). The active aluminum content of the "as received" nanometer aluminum was generally around 77–79%. The deionized water was supplied by Electron Microscopy Sciences (Reagent A.C.S. catalog no. 22800-01). The water had a maximum of 0.01 ppm silicate (as SiO_2), a maximum of 0.01 ppm heavy metal (as Pb), and 10 ppm of residue after removal from the packaging container due to evaporation.

When the nAl particles (immediately removed from the shipping container) were mixed with the deionized water, a low-temperature slow oxidation reaction occurred at the aluminum surface, where ammonia evolved and was detected by smell. It was suspected that nitrogen could have been bound to the nAl particle surface during the manufacturing process and was displaced by oxygen after being exposed to the water, resulting in ammonia formation. To minimize this low-temperature oxidation during mixing and eliminate the generation of ammonia, nAl particles were aged in the ambient air for an extended period of time to attain a reference material for use in combustion studies. The process involved placing nAl particles in a large surface area aluminum sheet pan, which was placed on a vibration and stirrer plate and exposed to air at ambient conditions for a specified period of time. Thermogravimetric analysis (TGA) and differential scanning calorimetry (DSC) analyses were performed with a Netzsch STA449F1 TGA–DSC on the as received and further passivated nAl particles. Figure 1 shows typical results. The mass gain and thermal behavior are similar for all the samples. As observed previously in the literature, low-temperature exotherms exist below the melting temperature of aluminum (660.32°C) before high-temperature oxidation processes. The TGA curves show that the material with extended passivation has less active aluminum, as indicated by the slightly smaller mass weight gain after all the aluminum has been oxidized. Figure 2 shows the dependence of the

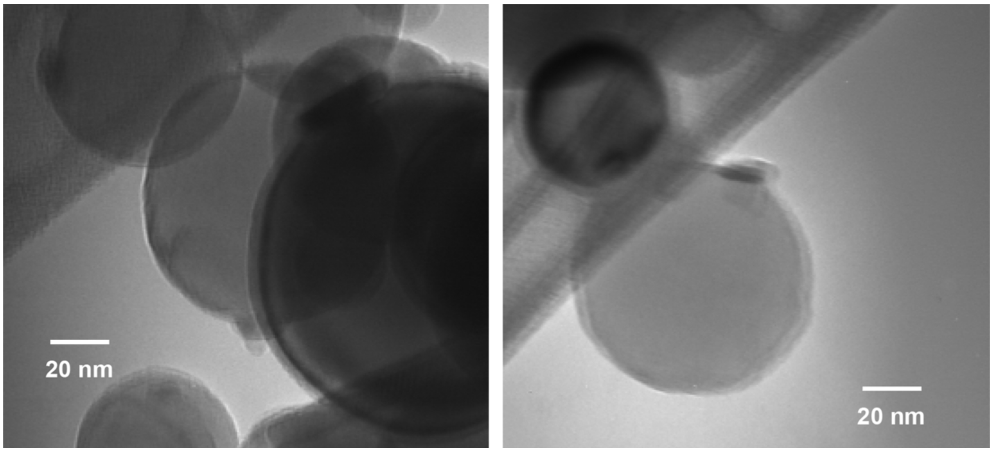

Fig. 3 TEM photographs of 80 nm Al particles without (left) and with (right) additional passivation.

Table 1 Relative concentrations of elements on a particle surface using XPS

Sample	Al, at.%	O, at.%	C, at.%	N, at.%	Si, at.%
38 nm	37.2	50.5	11.7	0.2	0.4
80 nm	34.6	42.0	21.4	1.2	0.8

Source: Malchi [25].

Table 3 Specific surface areas of 80 nm Al with and without extended passivation[a]

Time, h	Specific surface area, m^2/g
As received	26.6
120	23.7
>200	22.8

[a]The areas reported by the manufacturer were $\sim$26.1 m^2/g.

active aluminum content on the extended passivation time. The active aluminum content represents the pure aluminum contained in the particle. Figure 3 shows transmission electron microscopy images of the as received and further passivated particles. The oxide layer is clearly visible, although noticeable differences in the thickness are difficult to determine with the limited samples and magnifications. The particles are generally spherical, and the thickness of the oxide layer is nearly uniform.

To analyze the surface composition of nAl particles, Malchi [25] reported X-ray photoelectron spectroscopy (XPS) studies on two samples of nAl particles: 38 nm Al from Technanogy and the 80 nm Al used in this study from Nanotechnologies. A low-resolution survey scan was acquired from each specimen to identify the elements present. The relative concentrations and chemical states of these elements and organic and aluminum oxide overlayer thicknesses were determined from high-resolution scans acquired for O 1s, N 1s, C 1s, and Al 2p photoelectrons. The average sampling depth under these conditions was 40 Å (λAl2p). The results of the elemental analysis are summarized in Table 1.

The species observed on all samples included carbon species C-C, C-O, and COOR; amine; and SiO_2, Al_2O_3, and Al metal. The presence of nitrogen (in the form of amines) is noted to be greater on the 80 nm than on the 38 nm Al particles, which is consistent with the XPS studies of Sippel [30]. An energy dispersive spectroscopy (EDS) analysis was performed on the as received 80 nm Al particles and those that were passivated for 60 h (Table 2). Four different points (views) were analyzed for the as received sample, whereas three points were analyzed for the passivated samples. Results show good agreement with those from the XPS studies. Nitrogen is observed in the as received samples; it is not present in samples with extended passivation.

Surface areas of the as received and passivated 80 nm Al particles were measured by the Brunauer Emmett Teller method (Micromeritics Gemini Series). As summarized in Table 3, the surface area decreases with extended passivation, suggesting reduced reactivity due to increased oxide layer thickness and a lower active aluminum content. Generally, in the present experiments, a minimum passivation time of 48 h was applied. Once passivated, the aluminum was repackaged in argon to prevent any further changes in the particle characteristics before use.

B. Propellant Mixing and Sample Preparation

For all experiments, with the exception of several repeat experiments (described next), propellant mixing was performed by hand. The procedure included manually mixing the aluminum and water on a glass substrate while agitating the ingredients with a flat mixing spatula. Force was continuously applied to the mixture with the spatula to generate shear. Depending on the specific batch, the final material ranged from “claylike” to “solderlike.” The performance of the propellant was not significantly affected by the material state before freezing and testing.

Table 2 EDS analysis of 80 nm Al with and without additional air passivation

Element	View 1[a]	View 2	View 2[a]	View 3	View 1	View 2	View 3
	As received 80 nm Al, wt %				*Additional air passivation of 80 nm Al, wt %*		
N	0.11	0.23	0.43	0.42	0	0	0
O	0.12	0.11	0	0.4	0	0	0.39
Al	99.77	99.66	99.57	99.18	100	100	99.61
	As received 80 nm Al, at.%				*Additional air passivation of 80 nm Al, at.%*		
N	0.21	0.43	0.82	0.8	0	0	0
O	0.21	0.28	0	0.67	0	0	0.67
Al	99.6	99.37	99.18	98.53	100	100	99.34

[a]The different views represent different points of analysis across the particle sample.

Equivalence ratio ϕ was 0.71 for most of the mixtures studied, and the active aluminum content (for mixing purposes) was measured to be 74.5%. The amount of required oxidizer was determined based on the stoichiometry, which is determined by the active aluminum content. For each batch, the aluminum (weighed and placed on the mixing plate first) and water were combined and hand mixed until homogenized. Because of the claylike or solderlike consistency, manual packing into molds was required. After the tube molds were packed, the material was placed in an explosion proof freezer and stored at −30 °C. Densities (1.44 ± 0.03 g/cm^3) of the propellants in the filled tube molds were obtained by measuring the fill volume and the propellant mass. It is worth noting that once the material was frozen no reactions were observed. In fact, experiments were performed on propellant samples that had been frozen for several months, and no degradation in the performance was observed.

To verify mixing techniques, a number of experiments were conducted with a machine-mixing process using the Resodyn LabRAM® acoustic mixer. The Resodyn LabRAM mixes all phases, sizes, or ingredients without the use of any type of impeller. The acoustic mixer applies a uniform shear force throughout the mixture without delivering a significant amount of heat to the ingredients; it has an acceleration range from 0 to 100 Gs at frequencies between 58 and 68 Hz. The mixer has the capability of batch sizes of up to 500 g and can operate under vacuum. Using this mixer reduced the overall mixing time 10 fold. The 80 nm aluminum particles and deionized water were combined (unmixed) in a sealed container, which was encapsulated in a slightly larger container. Chilled water filled the void between inner and outer containers to reduce any heat generated during mixing. A preprogrammed mixing routine sequenced the mixer through a 20 s ramp from 0 to 40 Gs, then a constant mix cycle lasting 80 s at 40 Gs, and finally a reduced 20 G mix of 20 s duration before returning to 0 Gs.

For baseline comparisons of the ALICE propellants, two composite propellants were examined consisting primarily of AP (oxidizer) and HTPB (binder/fuel). The specific compositions are listed in Table 4. Ingredients were procured from Firefox Enterprises. The aluminum, with a nominal diameter of 20 μm, was obtained from Sigma–Aldrich. Both the aluminized and nonaluminized composite propellants were mixed using conventional mixing methods.

The binder/fuel, plasticizer, and bonding agents were combined initially with the catalyst and mixed to homogeneity. The oxidizer was then slowly introduced into the solution and hand mixed between additions to prevent air dispersion and maintain homogeneity until the polymer–solids mix became too viscous. At this point, the mixture was agitated by a mechanical mixer at a low speed to finish blending in the oxidizer. Subsequent to all ingredients being added to the mixture (except the curing agent), the blend was mixed in three 15 min intervals, scraping the mixing bowl walls between each interval and periodically during mixing. These prolonged mixing cycles aided in reducing heat generation and minimized the possibility of air being whisked into and trapped by the mixture. Once the polymer mix was thoroughly mixed, the curing agent was

Table 4 Formulations of the baseline nonaluminized and aluminized composite propellants

Ingredient type	Ingredient name	Nonaluminized formulation (solids loading 75.25%), wt %	Aluminized formulation (solids loading 82.03%), wt %
Oxidizer	Ammonium perchlorate (200 μm)	74.00	70.89
Binder/fuel	R45-M resin (HTPB)	14.00	10.13
Metal fuel	Aluminum (20 μm)	0.00	10.13
Plasticizer	2-ethylhexyl acrylate (EHA)	6.50	5.06
Catalyst	Ferric oxide (Fe_2O_3)	1.25	1.01
Bonding agent	HX-878 (tepanol)	0.75	0.76
Curing agent	Isonate 143-L (MDI)	3.50	2.03

introduced, and a 5 to 10 min postmix cycle completed the mixing process of the composite propellant.

Before grain casting, the propellant was placed into a vacuum oven at ambient temperature for 15 min to undergo degassing to remove entrapped gas. Once the curing agent was added, the working time was controlled by the amount of the curing agent and temperature of the mix. Small deviations in the amount of curative may have drastic effects on the curing time and propellant chain extension. The consistency of the nonaluminized propellant was pourable and could be flowed under vibration into prepared molds. The simultaneous vibration and pouring process minimized air entrapment during the packing process. The grains were then cured at 50°C for 24 to 48 h. The fully cured propellant was firm (not tacky or sticky), yet yielded under slight pressure (neither hard nor brittle). The aluminized propellant mixing process was similar to the nonaluminized composite, with the aluminum being introduced to the mix before the AP oxidizer. To assist the binding and coating of the aluminum particles within the mix and prevent any hazardous reaction with the AP oxidizer during mixing, the Al particles were precoated with a thin layer of turpentine before being added to the mix. Because of the higher solids loading, the aluminized composite propellant was more viscous than the nonaluminized polymer and typically required manual packing into the molds rather than pour filling. The densities of the nonaluminized and aluminized composite propellants were 1.55 ± 0.03 and $1.65 \pm 0.05\ \mathrm{g/cm^3}$, respectively.

C. Strand Burner Experiment

Steady-state strand burner experiments were performed to study the combustion mechanisms in a chamber constructed from 316 stainless steel; the chamber has four optical viewing ports, each having a 15.2 by 2.54 cm field of view. Feedthroughs in the baseplate were provided to allow both electrical signal and gas pathways into the chamber. The 61 cm long chamber had an inner diameter of 22 cm and a total free volume of 23 L to minimize the pressure variation caused by the generation of gaseous combustion products during an experiment. One of the optical viewing ports was backlit through an optical diffuser, whereas the opposite viewing port from the diffuser was used for real-time recording of the burning process by a Sony digital video camera. The operating pressure was varied from 0.8 to 15 MPa. The initial propellant temperature for the composite propellants was 25°C, and the ALICE samples were preconditioned at approximately −30 °C. Argon was used as the pressurant gas, and a Setra 206 pressure transducer was used to measure the instantaneous chamber pressure. Ignition was achieved by igniting a double-base propellant (NOSOL 363) by a resistance wire. A more detailed description of the experiment can be found in [4].

In total, three types of solid propellants were studied: 1) ALICE, 2) nonaluminized composite (AP–HTPB), and 3) aluminized composite (AP–HTPB–Al) propellants. The burning rate was characterized as a function of pressure and expressed in the form of the classical Saint Robert's law correlation. The sample was ignited at a specific pressure. Distance versus time curves were constructed from the recorded video, and the burning rate for that specific pressure was obtained from the slopes of the curves. The aluminum–water mixtures were packed in 8 mm inner diameter quartz tubes before freezing. The samples were tested frozen in the quartz tubes. The composite propellants were packed into the same 8 mm inner diameter quartz tubes and cured.

D. Solid-Propellant Motors

A series of three laboratory-scale motors with combustion chamber diameters of 1.91, 3.81, and 7.62 cm (0.75, 1.5, and 3 in.) were fabricated to evaluate the performance and scaling characteristics of the ALICE propellants. The motors were operated in both end burning and CP grain configurations. Nominally, for each configuration and motor diameter, a postcombustion chamber with a length of 7.62 cm was used. This left room for propellant grain lengths up to 25 cm. For CP motors, the grain length was kept constant at 7.62 cm, whereas for end burning grain motors 3.81, 7.62, and 15.24 cm lengths were studied. A schematic diagram (CP configuration) and a photograph of three different motors are given in Fig. 4. Two Setra pressure transducers were employed to monitor the pressures near the postcombustion chamber region. A custom-made rupture assembly with a 1.27 cm throughport was installed to prevent any overpressurization. Each motor chamber was hydrostatically tested at 1.5 times the working pressures. Specifically, the 7.62 cm motor was tested to 58.7 MPa (8515 psia) to enable the possibility of higher combustion pressures if warranted.

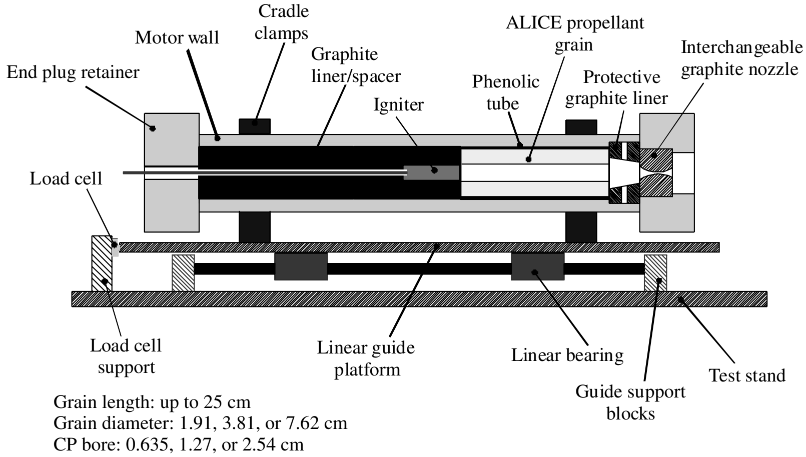

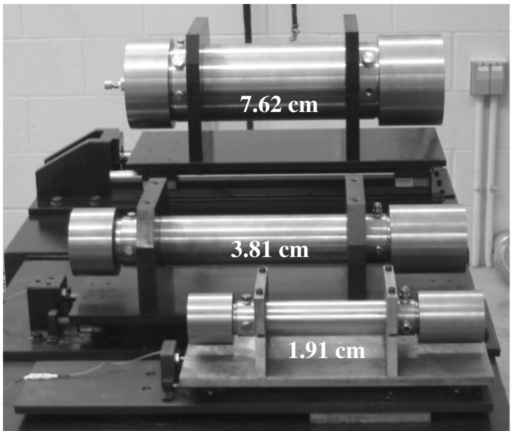

Fig. 4 Schematic diagram and photograph or three motors with CP grain configuration: 1.91, 3.81, and 7.62 cm in diameter.

Each motor has the capability of housing different precut nozzles to regulate pressure and propellant cast into phenolic tubes. The graphite nozzles had conical converging and diverging sections. The latter had a contraction ratio of 10 and a divergence half-angle of 15 deg. Ignition was achieved using a commercially available Estes or Aerotek model rocket, which was initiated with a small squib, which required a 5 to 12 V dc input. An appropriate OMEGA load cell was used (110, 440, and 2224 N) to determine the instantaneous thrust of the motor. Data were recorded at 5 kHz using a custom LabVIEW data acquisition program. The assembly and disassembly of the motor required virtually no tooling. The grain was cartridge loaded and followed by a nozzle holder plug, which used a piston-type seal. An end-retainer cap was threaded to secure the grain, postcombustion chamber, and nozzle in their respective locations.

Performance parameters such as combustion efficiency (η_{C*}) and specific impulse efficiency (ηI_{sp}) were determined by comparing the experimental measurements with the results of theoretical calculations performed at the same experimental operating conditions.

III. Results and Discussion

A series of experiments was conducted to characterize the ignition and burning behaviors of the ALICE propellants using both a constant-volume strand burner and various sizes of laboratory-scale solid rocket motors as functions of pressure, nozzle diameter, and grain geometry. Based upon chemical equilibrium calculations, two equivalence ratios were examined: $\phi = 0.71$ and 0.943. As expected, equivalence ratios near unity yielded the highest adiabatic temperatures but did not produce higher specific impulse compared with the fuel lean case. In fact, the specific impulse at $\phi = 0.71$ was 3% higher than for the case of $\phi = 0.94$, despite a lower adiabatic flame temperature. Based upon theoretical calculations, an equivalence ratio of 0.71 was chosen as the baseline case to yield less difficulty in mixing and forming strands and solid grains due to the excess water in the mixture.

A. Burning Rates

Figure 5 shows a series of video images of ALICE burning at a pressure of 3.55 MPa and an equivalence ratio of 0.71. Time zero corresponds to the instant just after the sample was ignited. The propellant exhibited a nearly one-dimensional burning front as the flame steadily propagated downward to the end. A luminous flame appeared always to be attached to the burning surface of the propellant strand. Figure 6 shows the burning rate as a function of pressure for ALICE at $\phi = 0.71$, yielding a pressure exponent of 0.79 for the hand-mixed samples. The densities of the Resodyn-mixed strands (1.48 g/cm^3) were very close to those obtained by hand mixing (1.44 g/cm^3). Consequently, the linear and mass burning rates of different samples are in good agreement. Equilibrium

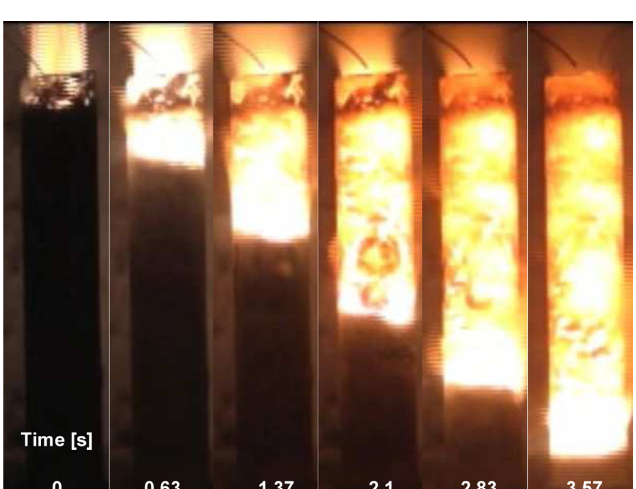

Fig. 5 Images of an 80 nm Novacentrix ALICE mixture combusting at 3.55 MPa and an equivalence ratio of $\phi = 0.71$.

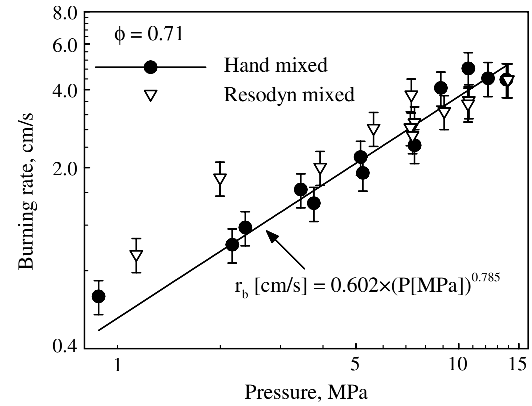

Fig. 6 Linear burning rate of the 80 nm ALICE mixture as a function of pressure for an equivalence ratio of $\phi = 0.71$. Both hand-mixed and machine-mixed results are presented.

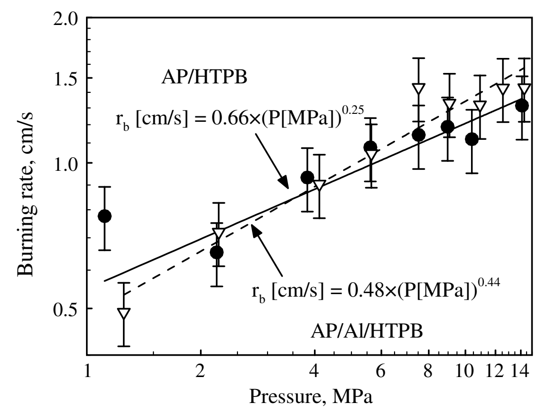

Fig. 7 Linear burning rate of nonaluminized and aluminized composite propellants as a function of pressure. The mixture formulations are given in Table 4.

calculations indicate that the combustion products of frozen propellants contain a mixture of solidified and liquid alumina for an equivalence ratio of 0.71. Figure 7 shows the linear burning rates for the two composite propellants. The nonaluminized AP–HTPB propellant has a pressure exponent of 0.25, and its metallized counterpart has a value of 0.44 for the range of pressures tested.

Figure 8 shows a comparison of the burning rates of nAl mixtures with ice and liquid water. The equivalence ratios were fixed at nearly one for both samples. The pressure exponent varies from 0.41 to 0.27 when the phase of the water is changed from a solid to a liquid form. The temperature of the Al–liquid water system is higher than the melting temperature of the oxide due to the absence of the heat of

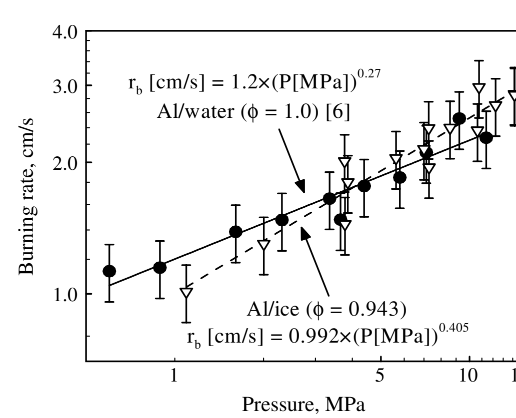

Fig. 8 Comparison of burning rates of nAl/ice ($\phi = 0.943$) and nAl/liquid water ($\phi = 1$) mixtures as a function of pressure for a particle size of 80 nm.

Table 5 Experimental results of the igniter characterization tests

Igniter type	Motor scale, cm	Peak thrust, N	Peak pressure, kPa	Nozzle throat, cm	Ignition stimulus effect, %
ESTES, A10-PT	1.91	<2.20	356	0.457	~2.5
ESTES, D12-0	3.81	<2.2	343	0.635	~1
Aerotek, G-80	7.62	~45	494	0.899	~8.5

fusion of ice. As a consequence of the change in slope, there is an inherent temperature sensitivity effect between the Al–water and ALICE mixtures. It is believed that the initial propellant temperature affects the prepower factor and not the pressure exponent. For ALICE propellants, both the prepower factor and the pressure exponent are affected. The burning rate for ALICE is lower than for Al–water, as additional energy is expended to increase the sensible enthalpy and melt the ice. The pressure exponent may be most affected by changes in the combustion efficiency. The decrease in temperature at lower pressures may result in a lower conversion efficiency, which would lower the temperature further and consequently indirectly increase the pressure exponent if the conversion efficiency increases at higher pressures. For example, Sabourin et al. [23] have previously reported a decrease in conversion efficiency for low pressures for fuel lean 38 nm Al–water mixtures ($\phi = 0.67$). Theoretical and experimental data suggest that the combustion of Al–water mixtures is diffusion controlled [4,6,31].

B. Thrust and Impulse

Static laboratory-scale motor test firings were performed with ALICE propellants at an equivalence ratio of 0.71 and with nonaluminized and aluminized AP–HTPB composite propellants. Comparisons of ALICE mixtures of $\phi = 0.71$ and 0.943 were examined by Connell et al. [28]. More than 100 tests were conducted using three different chamber diameters: 1.91, 3.81, and 7.62 cm (0.75, 1.5, and 3 in.). Both end burning and CP grain configurations were examined. For the CP grains, the inner grain diameters for the 1.91, 3.81, and 7.62 cm motors were selected as 0.635, 1.27, and 2.54 cm (0.25, 0.5, and 1 in.), respectively,

1. End Burning Grains

End burning experiments were performed to compare the steady-state strand burning rates with quasi-steady-state motor burning rates. Grain lengths ranging from 1.91 to 15.24 cm (0.75 to 6 in.) were tested in both the 1.91 and 3.81 cm motors. It was found that ignition was very difficult to achieve unless the following two criteria were met: 1) the pressure in the combustion chamber exceeded ~2–3 atm (40 psig) and 2) a sufficient duration of thermal heating was provided to allow for enough thermal energy to be transferred to the propellant surface. When poor ignition took place, the motor virtually became a low-pressure hydrogen generator, in which hydrogen gas exited the nozzle for several minutes as the reaction front propagated through the propellant grain. A 4.5 s end burning experiment was compared with a typical strand test at approximately the same pressure conditions. This test employed a 15.24 cm long ALICE grain in the 3.81 cm motor having a 0.325 cm diameter nozzle. Once the ALICE grain was fully ignited, the pressure reached 7 MPa (1015 psia) and quickly equilibrated to a quasisteady burning process. The thrust profile followed the pressure closely, indicating that there was no mechanical influence of the thrust stand on the measurements. A slight variation in pressure of periodic form during the quasisteady portion of the propellant burning was observed and attributed to transient accumulation of alumina on the nozzle surface due to the large amounts of alumina in the product gases. For the 4.5 s test, the average linear burning rate in the rocket configuration was estimated using an average pressure during the burn and equilibrium quantities. The average pressure for the experiment was 3.97 MPA (575 psia), resulting in an average burning rate of 1.7 cm/s, which is approximately 6% lower than the burning rate attained from strand burner experiments. Good agreement between the burning rates of the strands and the end burning grains showed no significant differences in burning behavior for a change in propellant diameter of nearly a factor of five. However, because of the large mass ratio of condensed phase products relative to gaseous products formed, entrainment of the aluminum particles due to the low surface area of the burning grain was not sufficient. CP grains with greater burning surface area (in the available motors) were studied to alleviate issues related to ignition and entrainment of aluminum from the propellant surface.

2. Center-Perforated Grains

Experiments were conducted using a CP grain to obtain high thrust levels. Because this configuration provides a large burning surface area, larger nozzles were warranted, and the influence of slag accumulation on the nozzle surface was reduced. Furthermore, a higher thrust level can be obtained for a reduced per-test grain mass. The burn time, however, is governed by the diameter of the grain rather than the length, and therefore a motor with a larger diameter is ultimately required. Ignition was achieved by using commercially available ESTES A10-PT and D12-0 and Aerotek G-80 solid-propellant rockets, which are readily available, cost effective, and well characterized. Because of the more demanding conditions for ALICE propellant ignition (high pressure and heat delivery), reliable and repeatable igniters were required. Each igniter in its respective motor was separately characterized so that similar pressures were achieved in each motor size before ALICE grain ignition. Test results are given in Table 5. The igniter size was increased with increasing motor scale due to the free volume of the chamber and the internal surface area of the propellant grain. Also in the table are data showing the enlarged impact of the igniter on the peak thrust of the motor. For the largest igniter, a maximum of 8.5% of the measured thrust resulted from the igniter. This percentage, however, was considerably lower in most cases.

Tests were also conducted to evaluate the influence of chamber pressure on ignition delay by using the same igniter (D12-0) in the 3.81 cm motor. The nozzle throat diameter was varied to change the pressurization rate and peak pressure associated with the igniter. Figure 9 shows the effect of the nozzle diameter on the ignition delay of the ALICE propellant grain. Although it is desirable to have a short ignition delay, the nozzle had to be chosen based upon the peak pressure in the motor. The ignition delay data for the 1.91 cm motor (not shown here) showed a similar trend.

In the process of scaling to larger motors, repeatability of motor test firings with CP grains was examined and verified. Figure 10 shows typical results (1.91 cm motor) demonstrating repeatability and a close-up view of the pressure-time profile, which is indicative of the progressive burn profile common to CP solid-propellant grains that possess continuously increasing burning surface areas. The

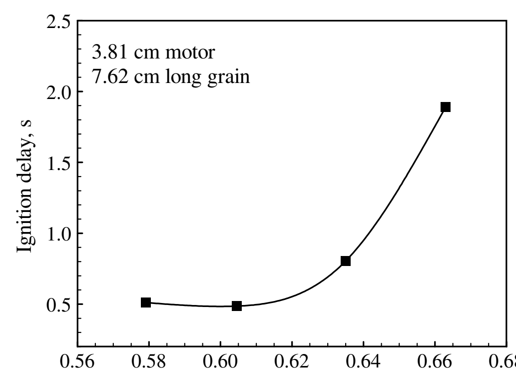

Fig. 9 Ignition delay for the 80 nm ALICE propellant in a 3.81 cm motor as a function of nozzle diameter.

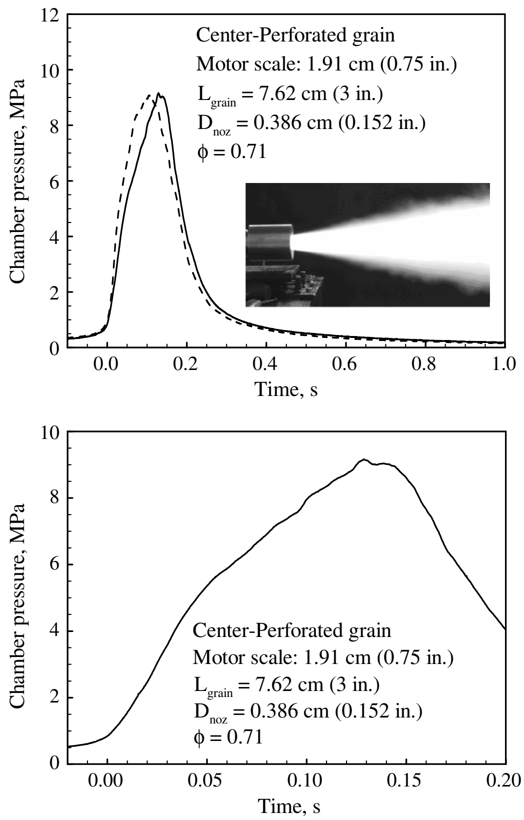

Fig. 10 Repeatability of the 1.91 cm motor test firings with CP propellant grains (top) and a magnified view of the pressure profile (bottom).

maximum chamber pressure reached approximately 9.1 MPa (1315 psia). The effect of motor orientation was also studied to verify that the horizontal static firings were representative of the conditions of vertical launches. The results for both orientations were very similar.

Figures 11 and 12 show the pressure and thrust profiles for four tests using the same ALICE grain configuration but different nozzles. As the nozzle diameter increases from 0.579 to 0.663 cm (0.228 to 0.261 in.), the pressure is reduced from 10.4 to 6.36 MPa (1515 to 937 psia). Although the pressure decreases with increasing nozzle diameter, the overall thrust remains approximately the same assuming the thrust coefficient does not vary because the area ratio was maintained at 10. This indicates that once a critical combustion pressure is achieved the performance is not significantly affected; this is as expected from the motor equation for thrust, $F = C_f P_c A_{th}$.

Figure 13 shows the results from a 7.62 cm motor firing. As expected, the thrust increased to nearly 908 N at the same chamber

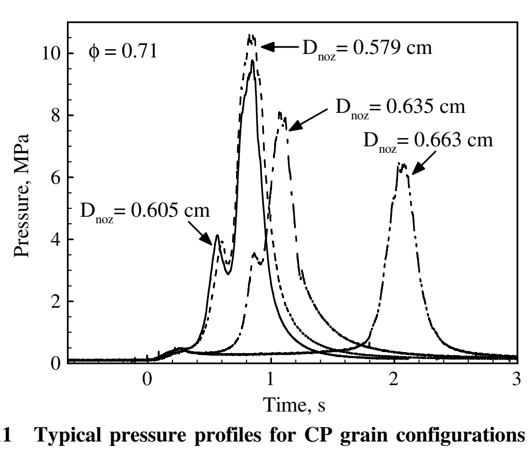

Fig. 11 Typical pressure profiles for CP grain configurations in the 3.81 cm motor using the ALICE propellant at $\phi = 0.71$. Time zeroed to ignition.

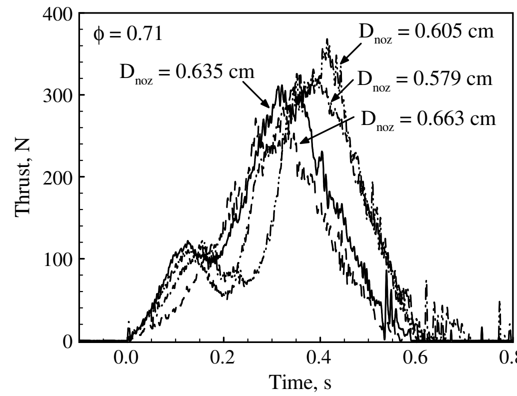

Fig. 12 Typical thrust profiles for CP grain configurations in the 3.81 cm motor using the ALICE propellant at $\phi = 0.71$. Time zeroed to start of thrust.

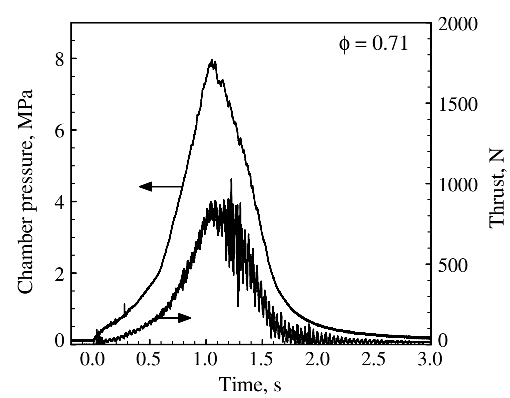

Fig. 13 Typical pressure and thrust profiles for CP grain configurations in the 7.62 cm motor using the 80 nm ALICE propellant at $\phi = 0.71$. Time zeroed to ignition.

pressure of around 8 MPa (1160 psia), compared with the 3.81 cm motor. The burning time for the 7.62 cm grain is slightly longer, due to the increased web thickness, and there was no noticeable ignition delay. It is evident that the igniter does not overpower the combustion process of the ALICE grain.

3. Motor Scaling

Scaling of the motor propulsive performance was performed in terms of geometric similarity and volumetric loading fraction (VLF). The latter is the ratio of the volume occupied by the propellant and the chamber free volume, excluding the nozzle. Typical VLFs range from 0.8 to 0.95 [32]. For all three motor chambers considered here, the loading fraction was 0.8 for the 7.62 cm long propellant grains. Figures 14 and 15 show the time histories of the pressure and thrust

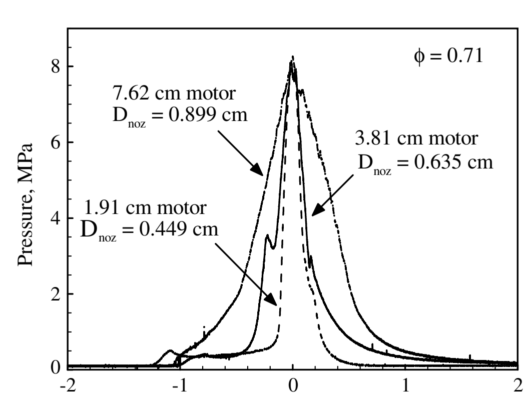

Fig. 14 Pressure profiles for the 1.91, 3.81, and 7.62 cm motors with the 80 nm ALICE propellants. Time zeroed to peak pressure.

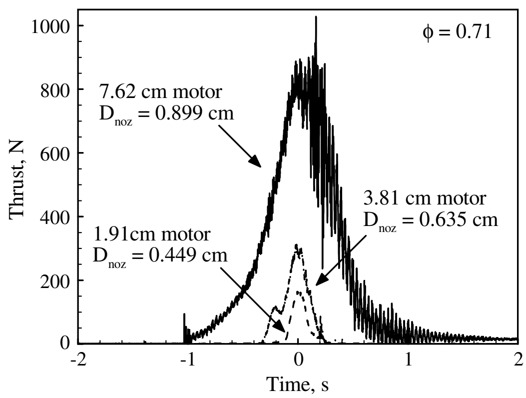

Fig. 15 Thrust profiles for the 1.91, 3.81, and 7.62 cm motors with the 80 nm ALICE propellants. Time zeroed as defined in Fig. 14.

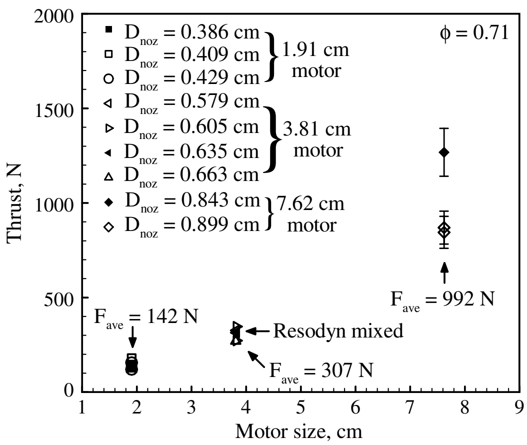

Fig. 16 Peak thrust obtained by scaling of 1.91, 3.81, and 7.62 cm motors having a 7.62 cm long CP 80 nm ALICE grain configuration and an equivalence ratio of 0.71.

profiles of ALICE propellants, respectively. The pressure profile of the 7.62 cm motor exhibited a broader distribution, which is indicative of a longer burning time (due to the increased web thickness). Because the length of the grain was fixed at 7.62 cm in these experiments, the initial CP surface area relative to the initial end-surface area decreased with increasing motor size. No significant change in burning mode (e.g., more end burning than CP burning) was observed based on the similarity in the thrust and pressure profiles between the three motors despite the largest motor having a length-to-diameter ratio close to unity.

The nozzle throat diameters for the 1.91, 3.81, and 7.62 cm motor nozzles were designed as 0.449, 0.635, and 0.899 cm, respectively, in order to achieve comparable pressures in the chambers. The peak thrusts for the 1.91, 3.81, and 7.62 cm motors were 166, 318, and 908 N, respectively. The peak thrust correlates with the surface area of the propellant for a given grain length, as shown by the data in Fig. 16. For each motor size, the test firing results were plotted individually, along with the average value. In the figure, each data point corresponds to a specific nozzle diameter for a particular motor size. According to the geometric scaling, the thrust should scale with the mass burning rate of the propellant, which is linearly dependent on the surface area. If the thrust is expressed by $F \sim a(D)^n$, then the ideal scaling is achieved when $n = 1$ and a is a constant. For the current tests, $n = 1.4$, which suggests that appreciable losses may still exist in the 7.62 cm motor.

Total impulse is the product of thrust and burning time. It amounts to the momentum that a given chemical system can yield. Figure 17 shows the total impulses for the three different sized motors. The thrust level increases with motor size. For the 1.91 cm motor, the total impulse is approximately $25\ \mathrm{N \cdot s}$. When the grain diameter was

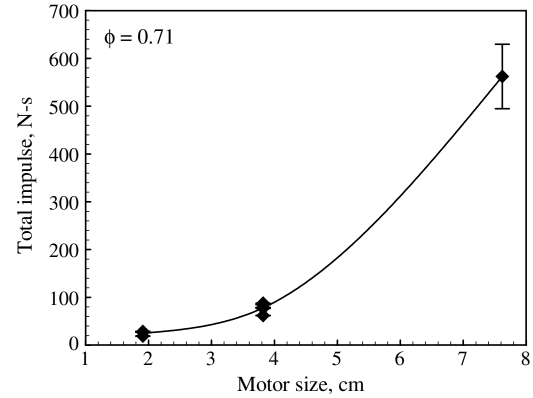

Fig. 17 Total impulses of motors with different sizes for 80 nm ALICE propellants.

increased by a factor of four to 7.62 cm, the total impulse increased by a factor of around 22.

The specific impulse was difficult to quantify in the present study, due to uncertainties in the determination of the propellant mass burning rate, which is varied during the experiment (because of surface area) and mass accumulation in the chamber. In the present study, the remaining mass left in the chamber was collected after each experiment and weighed to determine the amount of mass ejected from the nozzle (see Table 6). Typical percentages of residual mass ranged from 20 to 43%.

Several factors affect the variation of mass accumulated in the chamber during the test. Independent of scale, the postcombustion chamber length was kept constant at 7.62 cm. The benefit of this postcombustion cavity is to promote further mixing and reaction before the nozzle exit. The drawback to this extra reaction chamber is that it can allow mass to accumulate and be isolated from the product gas flow. Removing this chamber may reduce the accumulation of molten combustion products in the combustion chamber, but it may also sacrifice some combustion efficiency by reducing the residence time of the reactants in the chamber. These tradeoffs should be further studied.

Table 7 summarizes the performance parameters for the ALICE propellant. The measured specific impulse increased with motor size. The value, however, is lower than its theoretical counterpart, determined by the NASA Chemical Equilibrium Code [33] using the actual experimental test conditions as input. The I_{sp} efficiencies for the ALICE propellant increased from 27 to 64%, when the motor size increased from 1.91 to 7.62 cm (0.75 to 3 in.). The combustion efficiencies in the laboratory-scale rocket motors ranged from 43 to

Table 6 Mass remaining in the motor chamber subsequent to a hot firing

Motor scale, cm	Average mass retained, %
1.91	20.28 ± 14.69
3.81	29.44 ± 3.65
7.62	43.15 ± 1.06

Table 7 Performance parameters for ALICE propellants at an equivalence ratio of 0.71

	Value		
Parameter	1.91 cm motor	3.81 cm motor	7.62 cm motor
Peak thrust, N	166	318	908
$\bar{C}^*$, m/s	528	784	848
$\eta_{\bar{C}^*}$, %	43	64	69
$\bar{I}_{sp}$, s	56	83	133
$\eta_{\bar{I}sp}$, %	27	40	64
I_{sp} at peak pressure, s	97	124	203
$\bar{I}_{sp}$ with Al_2O_3 retained, s	63	117	233

69%, indicating that the poor combustion efficiency was responsible for the low specific impulse. According to previous work by Risha et al. [6], the combustion efficiency for an 80 nm Al–water strand in a closed volume was greater than 80%, and for ALICE the combustion efficiency was ∼69%. If the data at the maximum thrust or equivalently the maximum pressure are used to determine the I_{sp}, and the assumed burning surface area has a value based on 90% of the outer grain diameter, the estimated I_{sp} would be 97, 124, and 203 s for the 1.91, 3.81, and 7.62 cm motors, respectively. Because the burning-rate and combustion-efficiency data suggest that higher pressures are beneficial for propulsive performance, these conditions might be expected if the motor is designed to operate at high pressures for a longer period of time. The decreased combustion efficiency is a result of the low combustion temperatures for lean equivalence ratios (where solid-phase alumina may inhibit combustion), insufficient residence time for complete aluminum oxidation, and possible agglomeration of nanoaluminum at the propellant surface. Experiments show that the combustion efficiency increases with motor scale. The combustion efficiency for $\phi = 0.71$ was 43% for the smallest rocket motor. Despite the suggestion from theoretical calculations that the propulsive performance for mixtures with an equivalence ratio of 0.71 would outperform mixtures with nearly stoichiometric proportions ($\phi = 0.943$), experimental research conducted by Connell et al. demonstrated that the mixtures with $\phi = 0.943$ had higher combustion and specific impulse efficiencies [28].

The calculated specific impulse values were based upon the assumption that all of the mass was ejected out of the nozzle. However, if the alumina remaining in the chamber was considered as not exiting the nozzle, then the specific impulse values would be higher, as shown in Table 7. HTPB–AP composite propellant motor performance results suggest efficiencies increased with motor scale to approximately 90%. Although this suggests the 7.62 cm motor may be sufficient to characterize composite propellants, further scaling may ameliorate the low efficiencies exhibited by the ALICE propellant.

IV. Conclusions

ALICE propellants were successfully manufactured and tested in the strand burner and motor configurations. All experiments were conducted with Al particles with a nominal diameter of 80 nm. An equivalence ratio of 0.71 was considered for both strand burner and laboratory-scale rocket experiments. The linear burning rates of ALICE propellants exhibited a pressure exponent of 0.785 at an equivalence ratio of 0.71. ALICE propellant grains, in end burning and CP configurations, were also tested in laboratory-scale motors at an equivalence of 0.71. The nozzle diameter was systematically increased from 0.58 to 0.66 cm to analyze the effect of the chamber pressure on the ignition delay. The ignition delay increased with increasing nozzle diameter, although the overall thrust was not significantly affected by the nozzle diameter. The thrust increased from 166 to 908 N, as the motor size increased from 1.91 to 7.62 cm. The specific impulse also increased with increasing motor size from 56 to 133 s. The CP grain configuration featured a short duration of high-pressure combustion, leading to lower efficiencies. Combustion efficiencies ranged from 43 to 69% with increasing motor scale. Based upon the experimental data shown in this study, ALICE formulations in their current form are not viable for practical propulsion applications. However, these simple two-component systems offer very rich opportunities for fundamental scientific research.

Acknowledgments

The authors would like to thank the U.S. Air Force Office of Scientific Research and NASA for their sponsorship of this program under contract no. FA9550-07-1-0582. The authors would also like to thank Timothee L. Pourpoint, Steven F. Son, Tyler D. Wood, and Mark A. Pfeil from Purdue University for their contributions. Special thanks go to Rob Uhlig, Bryan Sones, and Lynn Witherite of the Applied Research Laboratory (ARL) at Pennsylvania State University for their assistance and usage of the Pennsylvania State University ARL test cell facilities. The efforts of Steven Dean for conducting the thermogravimetric analysis and differential scanning calorimetry experiments, Matthew Loomis for performing the energy dispersive spectroscopy tests, and Jeff Gesner for performing Brunauer Emmett Teller and transmission electron microscopy analyses are greatly appreciated.

References

[1] Greiner, L., "Selection of High-Performance Propellants For Torpedoes," *ARS Journal*, Vol. 30, No. 12, 1960, pp. 1161–1163. doi:10.2514/8.5354

[2] Greiner, L., *Underwater Missile Propulsion*, Compass, Arlington, VA, 1967.

[3] Ivanov, V. G., Gavrilyuk, O. V., Glazkov, O. V., and Safronov, M. N., "Specific Features of the Reaction Between Ultrafine Aluminum and Water in a Combustion Regime," *Combustion, Explosion, and Shock Waves*, Vol. 36, No. 2, 2000, pp. 213–219. doi:10.1007/BF02699363

[4] Risha, G. A., Son, S. F., Yetter, R. A., Yang, V., and Tappan, B. C., "Combustion of Nano-Aluminum and Liquid Water," *Proceedings of the Combustion Institute*, Vol. 31, No. 2, 2007, pp. 2029–2036. doi:10.1016/j.proci.2006.08.056

[5] Connell, T. L. Jr., Risha, G. A., Yetter, R. A., Young, G., Sundaram, D. S., and Yang, V., "Combustion of Alane and Aluminum with Water for Hydrogen and Thermal Energy Generation," *Proceedings of Combustion Institute*, Vol. 33, No. 2, 2011, pp. 1957–1965. doi:10.1016/j.proci.2010.07.088

[6] Risha, G. A., Sabourin, J. L., Yang, V., Yetter, R. A., Son, S. F., and Tappan, B. C., "Combustion and Conversion Efficiency of Nano Aluminum–Water Mixtures," *Combustion Science and Technology*, Vol. 180, No. 12, 2008, pp. 2127–2142. doi:10.1080/00102200802414873

[7] Foote, J. P., Lineberry, J. T., Thompson, B. R., and Winkelman, B. C., "Investigation of Aluminum Particle Combustion for Underwater Applications," AIAA Paper 1996-3086, 1996.

[8] Ingenito, A., and Bruno, C., "Using Aluminum for Space Propulsion," *Journal of Propulsion and Power*, Vol. 20, No. 6, 2004, pp. 1056–1063. doi:10.2514/1.5132

[9] Lee, W. M., "Aluminum Powder–Water Reaction Ignited by Electrical Pulsed Power," U.S. Naval Surface Warfare Center, Rept. AD-A269223, 1993.

[10] Kravchenko, O. V., Semenenko, K. N., Bulychev, B. M., and Kalmykov, K. B., "Activation of Aluminum Metal and Its Reaction with Water," *Journal of Alloys and Compounds*, Vol. 397, Nos. 1–2, 2005, pp. 58–62. doi:10.1016/j.jallcom.2004.11.065

[11] Miller, T. F., and Herr, J. D., "Green Rocket Propulsion by Reaction of Al and Mg Powders and Water," AIAA Paper 2004-4037, 2004.

[12] Lo, R. E., Adirim, H., and Poller, S. "Cryogenic Solid Propulsion Technology Development Status," AIAA Paper 2004-3477, 2004.

[13] Adirim, H., Lo, R. E., Pilz, N., Schöyer, H., Gläser, S., Weiser, V., Noack, E., Meusemann, H., and Caramelli, F., "Cryogenic Solid Propulsion Technology Development Status," AIAA Paper 2005-4093, 2005.

[14] Adirim, H., Lo, R. E., Pilz, N., Schöyer, H., Gläser, S., Weiser, V., Noack, E., Meusemann, H., and Caramelli, F., "State-of-the-Art in Solid Propulsion Research," AIAA Paper 2006-4420, 2006.

[15] Franson, C., Orlandi, O., Perut, C., Fouin, G., Chauveau, C., Gokalp, I., and Calabro, M., "New High Energetic Composite Propellants for Space Applications: Refrigerated Solid Propellant (RSP)," *Progress in Propulsion Physics*, Vol. 1, 2007, pp. 31–46. doi:10.1051/eucass/200901031

[16] Franson, F., Orlandi, O., Perut, C., Fouin, G., Chauveau, C., Gokalp, I., and Calabro, M., "Al/H_2O and $Al/H_2O/H_2O_2$ Frozen Mixtures as Examples of New Composite Propellants for Space Applications," *7th International Symposium on Launcher Technologies*, Paper 5.01.04, Barcelona, 2007.

[17] Yetter, R. A., Risha, G. A., and Son, S. F., "Metal Particle Combustion and Nanotechnology," *Proceedings of the Combustion Institute*, Vol. 32, No. 2, 2009, pp. 1819–1838. doi:10.1016/j.proci.2008.08.013

[18] Huang, Y., Risha, G. A., Yang, V., and Yetter, R. A., "Combustion of Bimodal Nano/Micron-Sized Aluminum Particle Dust in Air," *Proceedings of the Combustion Institute*, Vol. 31, No. 2, 2007, pp. 2001–2009. doi:10.1016/j.proci.2006.08.103

[19] Huang, Y., Risha, G. A., Yang, V., and Yetter, R. A., "Effect of Particle Size on Combustion of Aluminum Particle Dust in Air," *Combustion and Flame*, Vol. 156, No. 1, 2009, pp. 5–13. doi:10.1016/j.combustflame.2008.07.018
[20] Puri, P., and Yang, V., "Effect of Particle Size on Melting of Aluminum at Nano Scales," *Journal of Physical Chemistry C*, Vol. 111, No. 32, 2007, pp. 11776–11783. doi:10.1021/jp0724774
[21] Puri, P., and Yang, V., "Effects of Voids and Pressure on Melting of Nano-Particulate and Bulk Aluminum," *Journal of Nanoparticle Research*, Vol. 11, No. 5, 2008, pp. 1117–1127. doi:10.1007/s11051-008-9505-x
[22] Puri, P., and Yang, V., "Thermo-Mechanical Behavior of Nano Aluminum Particles with Oxide Layers During Melting," *Journal of Nanoparticle Research*, Vol. 12, No. 8, 2010, pp. 2989–3002. doi:10.1007/s11051-010-9889-2
[23] Sabourin, J. L., Risha, G. A., Yetter, R. A., Son, S. F., and Tappan, B. C., "Combustion Characteristics of Nanoaluminum, Liquid Water, and Hydrogen Peroxide Mixtures," *Combustion and Flame*, Vol. 154, No. 3, 2008, pp. 587–600. doi:10.1016/j.combustflame.2008.05.015
[24] Sippel, T. R., Son, S. F., Risha, G. A., and Yetter, R. A., "Combustion and Characterization of Nanoscale Aluminum and Ice Propellants," AIAA Paper 2008-5040, 2008.
[25] Malchi, J. Y., "Combustion and Self-Assembly of Nanoenergetic Materials," Ph.D. Dissertation, Pennsylvania State Univ., University Park, PA, 2007.
[26] Wood, T. D., Pfeil, M. A., Pourpoint, T. L., Tjolus, J., Son, S. F., Connell, T. L. Jr., Risha, G. A., and Yetter, R. A., "Feasibility Study and Demonstration of an Aluminum and Ice Solid Propellant," AIAA Paper 2009-4890, 2009.
[27] Connell, T. L. Jr., "Combustion of Aluminum and Ice Based Solid Propellants for Propulsion Applications and High Temperature Hydrogen Generation," Master's Thesis, Pennsylvania State Univ., University Park, PA, 2011.
[28] Connell, T. L. Jr., Risha, G. A., Yetter, R. A., Yang, V., and Son, S. F., "Combustion of Bimodal Al and Ice Mixtures," *International Journal of Energetic Materials and Chemical Propulsion*, Vol. 11, No. 3, 2012, pp. 259–273.
[29] Risha, G. A., Connell, T. L. Jr., Yetter, R. A., Yang, V., Wood, T. D., Pfeil, M. A., Pourpoint, T. L., and Son, S. F., "Aluminum-Ice (ALICE) Propellants for Hydrogen Generation and Propulsion," AIAA Paper 2009-4877, 2009.
[30] Sippel, T. A., "Characterization of Nanoscale Aluminum and Ice Solid Propellants," Master's Thesis, Purdue Univ., West Lafayette, IN, 2009.
[31] Sundaram, D. S., Yang, V., Connell, T. L. Jr., Risha, G. A., and Yetter, R. A., "Flame Propagation of Nano/Micron-Sized Aluminum Particles and Ice (ALICE) Mixtures," *Proceedings of the Combustion Institute*, Vol. 34, No. 2, 2013, pp. 2221–2228. doi:10.1016/j.proci.2012.06.129
[32] Sutton, G. P., and Biblarz, O., *Rocket Propulsion Elements: An Introduction to the Engineering of Rockets*, 6th ed., Wiley, New York, 1992, pp. 447–452.
[33] McBride, B. J., and Gordon, S., "Computer Program for Calculation of Complex Chemical Equilibrium Compositions and Applications," NASA, Reference Publication 1311, 1996.

L. Maurice
Associate Editor